

17 Precision Temperature Control

J. Pecson,^{*} D. A. Boyd,[†] A. Hashemi,^{*} K. Aaron,[‡] J. Ambrose,^{**}
J. F. Maddox,[†] E. M. Mattison,[†] and R. F. C. Vessot[†]

Introduction

Tight control of payload or component temperatures to values on the order of 1°C has been routinely accomplished on many programs during the past few decades. In recent years, however, some civilian and military payloads have been developed that demand much more stringent temperature stability for precision optical systems and high-accuracy clocks. For optical systems, even milliKelvin (mK) changes in temperature can result in thermal deformations in the range of nanometers and picometers that can translate into unacceptable errors in the pointing accuracy of optical elements. The Space Interferometry Mission (SIM), the Next Generation Space Telescope (NGST), and the Terrestrial Planet Finder (TPF) are examples of state-of-the-art programs with such strict deformation requirements on optical surfaces. Even tighter temperature control can be required for time-reference clocks where temperature changes of only tenths of a milliKelvin can cause unacceptable drift in time measurement. The hydrogen maser clock (HMC) program is an example of a time-reference system with such demanding thermal-control requirements.

Given that an aluminum atom has a diameter on the order of 0.3 nanometers, maintaining the relative position of the optical elements on a spacecraft structure to subnanometer accuracy is quite a feat. Either the coefficient of thermal expansion (CTE) of the structure and mirror material must be extremely low or the temperature field needs to remain nearly constant—or a combination of these requirements must be met. These are difficult requirements on the materials, and therefore thermal-stability issues are clearly at the heart of programs like SIM, NGST, and TPF. To achieve temperature stability, the thermal designers of these programs have chosen to thermally isolate the temperature-sensitive components from external heating variations and then rely on thermal capacitance and conductance effects to dampen residual temperature changes to values on the order of milliKelvins.

For other programs, like HMC, highly stable temperatures are achieved by isolating sensitive components from changes in the external environment and then actively controlling temperatures to the submilliKelvin level. In this type of design, the focus changes from passive to active control, from control of temperature to control of heat-flow paths and gradients, and from thermostats to detailed behavior of control loops and their compensation. Focus is also placed on limitations on control arising from heater-sensor placement. Calibration of and among

^{*}Lockheed Martin, Palo Alto, California.

[†]Smithsonian Astrophysical Observatory, Cambridge, Massachusetts.

[‡]Jet Propulsion Laboratory, California Institute of Technology, Pasadena, California.

^{**}Lockheed Martin, Sunnyvale, California.

nearly identical sensors, self-heating by measurement current, and resistance changes of lead wires become important. Electrical and thermal aspects of the control system become less separable, and local temperature sensitivity of the electronic control system can be critical. Long-term stability of sensors and electronics alike can limit design choices if control is required for months or years.

In this chapter, an overview of the SIM thermal-design philosophy and requirements is given to highlight the challenges of precision temperature control of optical systems. For this class of problem a methodology for multidisciplinary modeling is presented, and prediction and validation of a milliKelvin-level optical test bed are discussed. Similarly, the thermal design and test verification of the HMC are used to illustrate the thermal-design issues for active submilliKelvin-level temperature control at the component level.

The Space Interferometry Mission

To explore the issues of spacecraft-level precision temperature control, we begin with a description of SIM and its mission and thermal challenges. The SIM is an independent and essential stepping-stone within NASA's Origins Program. SIM will determine the positions and distances of stars several hundred times more accurately than any previous program. This accuracy will allow SIM to determine the distances from Earth to stars throughout the galaxy and to probe nearby stars for Earth-sized planets. SIM is a joint effort of the Jet Propulsion Laboratory (JPL), California Institute of Technology, Lockheed Martin Missiles and Space, and TRW.

The SIM flight system (Fig. 17.1) consists of the interferometer instrument system and the spacecraft system. The instrument system consists of the optics, actuators, sensors, and computers needed to make science observations. The spacecraft system provides the essential engineering functions for flight operations, including the structure, power subsystems, attitude control, propulsion, communication, and thermal control.

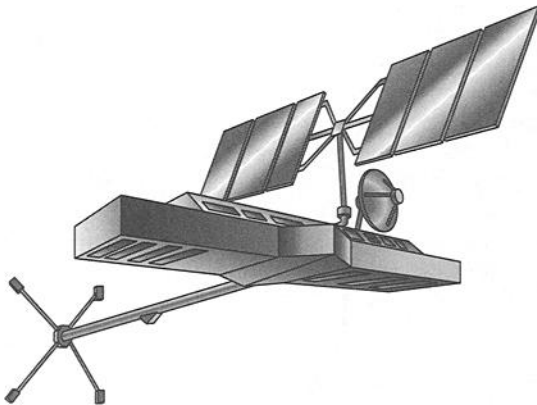


Fig. 17.1. The SIM flight system.

The SIM instrument (Fig. 17.2) operates by collecting starlight using pairs of small telescopes and combining the light onto sensitive CCD (charge-coupled device) detectors to create constructive interference. When all elements are carefully aligned, very precise measurements made using a laser interferometric metrology system, coupled with knowledge of guide star locations, can be used to establish the angular position of the target star or other celestial object.^{17.1}

SIM performs astrometry (measurement of star locations) by using a white-light Michelson interferometer with a 10-m baseline. Groups of optical elements (similar to telescopes) are located 10 m apart on opposite ends of a precision support structure (PSS) to collect the starlight, as shown in Fig. 17.2. Light from these telescope-like assemblies is combined in an astrometric beam combiner (ABC) in the middle of this large instrument. Optical delay lines (ODLs) are used to adjust the path length followed by the starlight so that the wavefronts from both arms of the interferometer arrive at the detector at precisely the same time. The path lengths within the instrument are then measured to a precision (not accuracy) of a few tens of picometers using infrared laser metrology gauges. Based on these measurements and other laser gauge measurements of the baseline length, the angle between the target star and the baseline is determined. To find the orientation of the astrometric baseline, two other similar astrometric interferometers are used. The baselines for all the interferometers are kept as parallel as possible. The laser metrology system measures the small amount of deviation from parallelism to make corrections to the results.^{17.2}

The SIM spacecraft will be launched from Cape Canaveral in 2009. In its orbit, the spacecraft will slowly drift away from Earth at a rate of approximately 0.1 AU

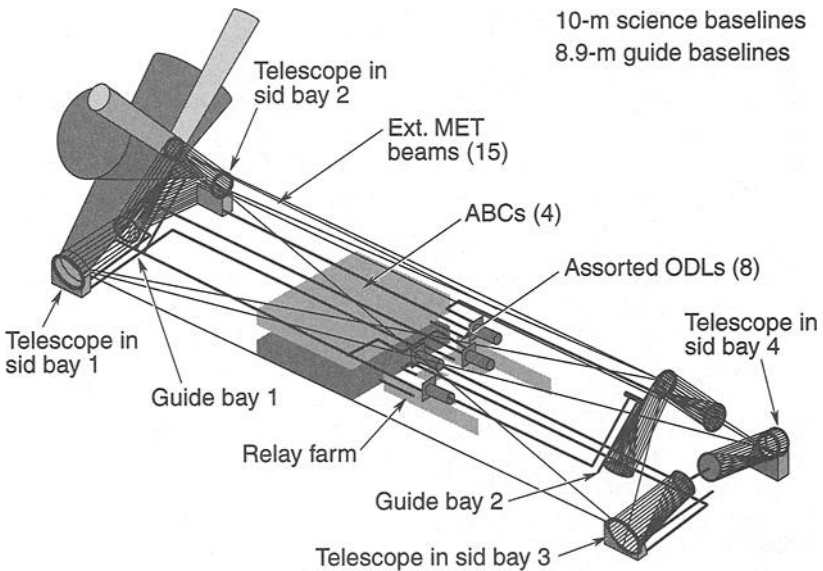


Fig. 17.2. The SIM instrument.

per year, reaching a maximum communication distance of about 95 million km after 5.5 years. In this Earth-trailing solar orbit the spacecraft will receive continuous solar illumination, avoiding the temperature swings caused by eclipses in an Earth orbit. This is one of the very few instances in which thermal-control requirements have actually dictated the choice of mission orbit!

Successful development of SIM requires that four “grand technological challenges” be overcome:

- nanometer-level control and stabilization of optical-element positions on a lightweight flexible structure
- subnanometer-level sensing of optical-element relative positions over meters of separation distance
- overall instrument complexity and the implications for interferometer integration and test and autonomous on-orbit operation
- picometer-level optical-deformation control and stabilization

Thermal Challenges and Design Approach

The challenging picometer-level optical requirements impose severe thermal and structural requirements on SIM. Its thermal-control subsystem technologies are designed to satisfy the stressing requirements on temperature stability and temperature gradients within the starlight-collecting optics and the instrument. Potential thermal disturbances to these subsystems include time-varying sun angles, on/off heater operation, optical-element position changes (slewing), heat pulses from cameras or actuators, and power variations in electronics units.

Thermally induced optical-path errors can arise from changes in the shape of the optics and changes in the shape of the structure that supports them. As an example, a 2.6-mK change in the front-to-back temperature difference of the compressor primary mirror during a 1-hr period will cause a 40-picometer error in the astrometric measurement.

Beam-walk errors occur because of the difference between the metrology and starlight optical paths. As long as this difference remains constant, the instrument can calibrate out the error. However, if the metrology-starlight difference varies as the instrument makes its observation, an error in the astrometric measurement will result. This difference can come from a number of sources. Thermally induced errors are a major source.

The overall design approach for the optics is to thermally isolate and minimize variations in the viewing temperature of the optics, as shown in Fig. 17.3. To meet this requirement, the view of exposed mirrors to space is maximized with each mirror having a heater plate radiating to its entire back and side surfaces to reduce and maintain stable gradients within the mirrors. The heater plate back and sides are enclosed in multilayer insulation (MLI). The enclosed optics are housed within 0.1-K-controlled bay walls and a precision support structure (PSS). Within this environment, the optics temperature can be stabilized to meet the milliKelvin stability required during data collection.

The thermal enclosures and the PSS employ multiple lightweight computer-controlled heaters and MLI blankets, as illustrated in Fig. 17.4. This thermal design cold-biases the PSS by using exterior surface components that are always colder than the desired operating temperature, even in direct sunlight. For the

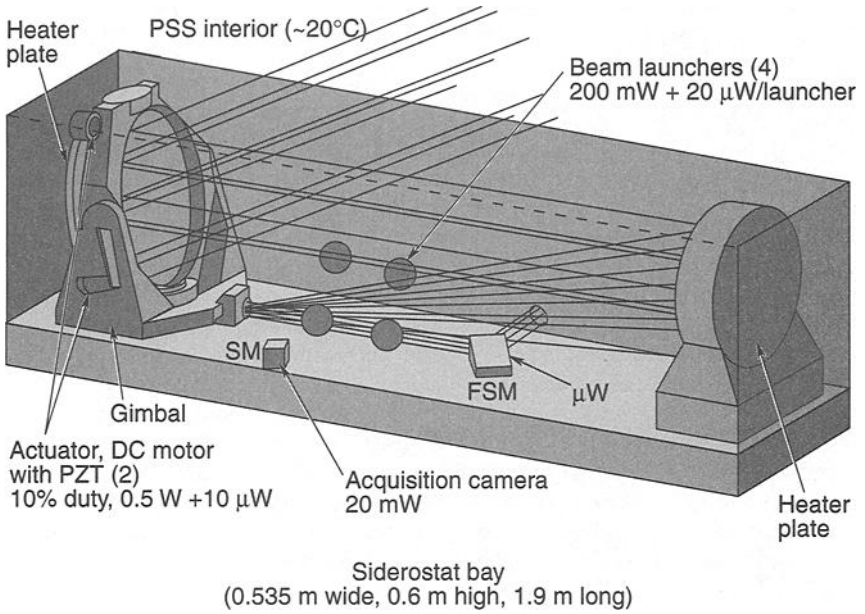


Fig. 17.3. Siderostat bay heat sources.

Cold-biased system

- Control temp > environment
- Positive heater control

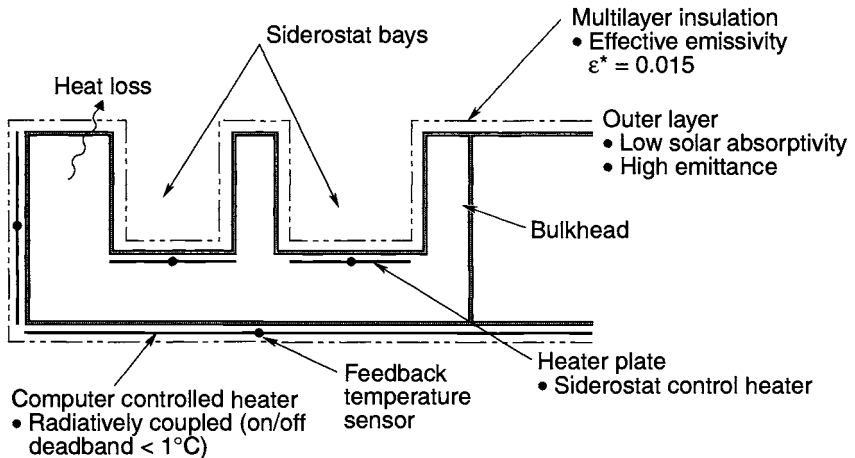


Fig. 17.4. PSS thermal control approach.

required five-year life, the cold-biasing objective would be achieved by using MLI with silvered-Teflon outer cover sheets. Heaters are controlled via the spacecraft computer, which sends on/off commands to the heater drive electronics.^{17.1}

Analysis Approach

Optical design, with deformation requirements in the nanometer and picometer range, often requires testing and prediction capabilities beyond the state of the art. In this context, integrated thermal-optical-mechanical modeling is essential to aid the design process, predict system performance, and assign error budgets to various components and subsystems. This section describes a methodology for performing integrated design and analysis for space optical systems using OPTIMA, an optical analysis code, and I-DEAS/TMG, an integrated CAD/CAM/CAE software package. This approach was found to streamline the process for obtaining accurate and reliable design information and to enhance prediction capability.

The conventional design approach to modeling such systems is a lengthy and cyclic process involving geometric modeling and a series of analyses, each focusing on a different physical discipline. The performance and cost of the final design depend on how effectively and quickly the designer can accommodate the requirements imposed by each of these disciplines. Integrated multidisciplinary modeling is a cost-efficient way to substantially reduce design time, provide system optimization, and generate accurate predictions.

The design and analysis process described in this section involves multiple disciplines and assumes that an individual designer/analyst performs each role. In actual practice any number of engineering specialists could contribute to each function. The methodology starts with an optical designer, who develops the optics to meet the science requirements. A structural designer then specifies additional hardware to maintain the position of the optical components. Once the design is complete, a thermal analyst develops a thermal-control scheme and predicts the thermal response of the design to confirm that it satisfies the temperature requirements. Subsequently, a structural analyst calculates the thermal deformations induced by the temperature gradients. Finally, these deformations are used as input by the optical analyst in characterizing the impact of the displacements on the image quality. Figure 17.5 illustrates steps in the design methodology, which the following sections explain in greater detail.

Methodology

Optical Design

The first step in designing and evaluating a space optical system is to define the optical elements it comprises. Once a starting configuration is developed from a set of requirements, Lockheed Martin's optical design and analysis program, OPTIMA (or a similar commercial optical analysis tool, such as MACOS, Code V, or Optix) is used to optimize the design.

Many options are considered in designing optical systems to meet requirements. Material selection can have a significant impact on performance. The optical designer's choice of materials with near-zero CTE at operating temperature reduces thermal deformations. Also, thermal gradient effects are minimized by use of materials with a high thermal conductivity.

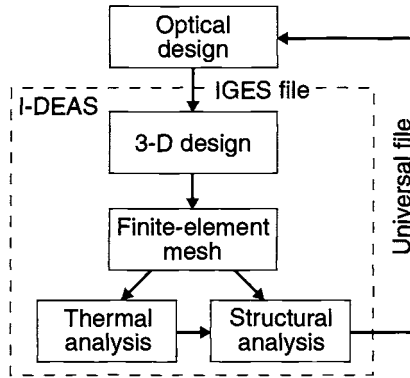


Fig. 17.5. Space optical-system design methodology.

Once the desired optical configuration is determined, the lens and mirror definitions with ray traces (light path) are translated by the optical designer into a series of Initial Graphics Exchange Specification (IGES) files for transfer to a structural designer.

Figure 17.6 shows a representative space optical system similar to that of one siderostat bay unit within the SIM spacecraft. The sequence of mirrors represents a beam collector (the siderostat mirror) and beam compressor (the primary mirror) with a focal point at 1.3 meters. The optical elements were created in OPTIMA and then imported into I-DEAS, via IGES files. The associated ray traces are also displayed in the figure. The light is collected by the siderostat mirror, which directs the starlight in a fixed outward direction toward the primary mirror and then through the remaining optical elements.

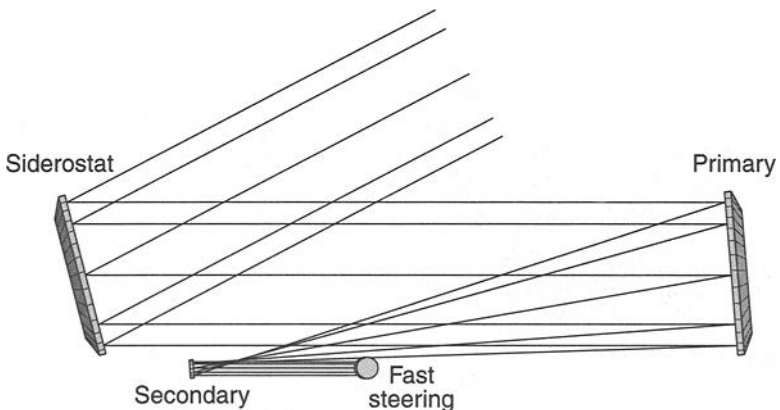


Fig. 17.6. Representative space optical system.

Structural Design

The IGES files from the optical designer are imported into I-DEAS, an integrated CAD/CAM/CAE software package for design and analysis of components and assemblies in a common environment. This commercial tool consists of various modules for design, drafting, assembly, meshing, and analysis. The graphical user interface and postprocessing module enable easy viewing of results, allowing rapid problem diagnosis and design evaluation.

The structural designer uses I-DEAS to create the support structure necessary to maintain the position of the components. This structure may include mirror mounts, an optical bench, and enclosure walls. Special care is given to the mirror mounts to ensure the force exerted on the optical components does not distort the optical surface. Designers strive to obtain high mounting stiffness to maintain optical element position. Other goals are ensuring mount size and weight are as small as possible and keeping costs low.

Once the support structure is created, various parts are grouped into logical levels of assembly, creating a hierarchy of all parts within a master assembly. For example, a mirror might belong to an instrument subassembly that (when coupled with the bus) comprises the satellite master assembly. A concrete example of the benefits this order creates will be presented in a subsequent section.

The materials for all parts, including optical components and support structure, are then incorporated into a material database within I-DEAS. Although the structural designer uses the software tool to apply material properties to each part, the optical designer is responsible for specifying the materials and surface coatings for all optical components.

Using the optics created in the previous step, the structural designer assembles a structure (Fig. 17.7) to precisely maintain the position of the optical components. The siderostat mirror gimbal is constructed to enable the mirror to rotate plus or minus several degrees to accommodate the science requirements. A mirror housing “wedge” and bipod flexure mount are created to support the primary mirror. Mirror mounts for the secondary and fast steering mirrors are also created. Finally, also shown in Fig. 17.7 is the optical bench. At this stage, material properties are associated with each part, and an assembly of the system is generated.

Thermal and structural analysts are able to take advantage of the data that has already been created by the structural designer, so the transition between analysis phases is easily made. Because of the common environment, information such as geometric dimensions, volumes, material properties, and assembly layout is automatically available to both thermal and structural analysts.

Finite-Element-Method (FEM) Mesh

Using the meshing module within I-DEAS, thermal and structural analysts generate FEM meshes depicting the optical system. Because the meshes are created in the same software environment in which the optical system was structurally designed, the analysts take full advantage of the geometry created in the previous step, eliminating redundancy. This significant process savings comes at a small cost. Typically some reduction to the solid model is necessary to ease the meshing process—not all features are required to perform an acceptable analysis. Features

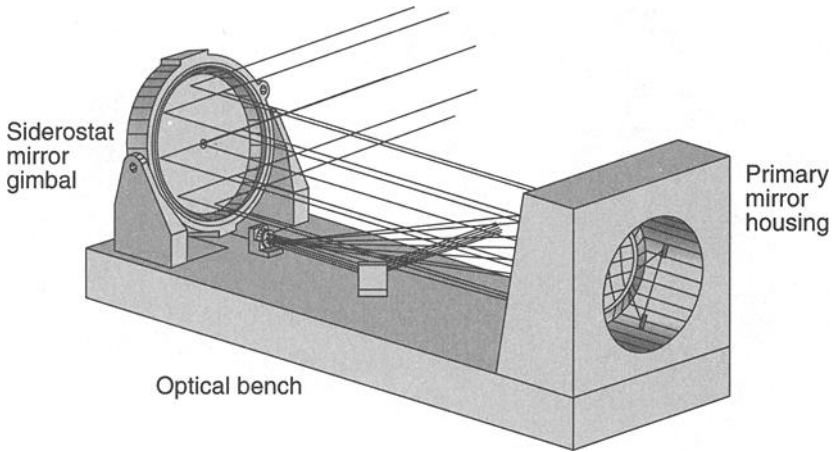


Fig. 17.7. Optics structure assembled to precisely maintain the position of the optical components.

such as fillets, bolt holes, and chamfers can be suppressed for the thermal or structural analysis, depending on the analysts' objectives. Suppressing such features is handled with utilities available in the software.

The mesh density of the model is related to the temperature resolution and deformation information required for the analysis. Each analyst is responsible for ensuring that the element types and mesh density used for a given component properly represent its thermal and structural behavior. Two meshes are typically created, one each for the thermal and structural analyses; however, in certain instances one is sufficient. If two are utilized, an automated temperature-mapping utility within I-DEAS maps temperatures from a thermal analysis onto a structural model using a local-element temperature function.

Another advantage of this integrated process is the ability to associate an FEM mesh with the solid geometry. This association enables the mesh to be updated when the geometry changes, which is particularly useful during early phases of design, when changes occur frequently. It also enables use of the assembly information generated by the structural designer. Parts occurring multiple times within an assembly are meshed once rather than repeatedly at each instance and correctly oriented into the proper locations. For example, an interferometer uses two identical telescopes to collect light. Using the solid geometry and taking advantage of the assembly information, the software meshes the first telescope's components, then automatically meshes the second telescope and orients it in the proper location.

Continuing with the example, we find an FEM mesh of the optical system is created (Fig. 17.8). Several of the parts are meshed individually and merged to form a system FEM mesh as shown in the figure. The assembly information created by the structural designer enables the correct placement of the parts in relationship to each other. Also, the material properties assigned to the 3-D solid geometry in the previous step are automatically associated to the mesh definitions for each part. (The mesh in Fig. 17.8 is not optimized to represent the mesh density

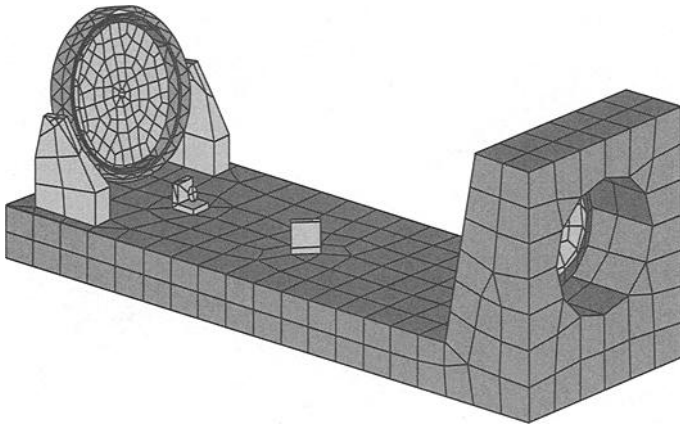


Fig. 17.8. FEM mesh of the optical system.

required to accurately capture milliKelvin-level deformation behavior required in the SIM mission. The figure is for demonstration purposes only.)

Thermal Analysis

Once the FEM mesh is completed, the thermal analyst defines the proper boundary conditions within the I-DEAS Thermal Model Generator (TMG). Thermal couplings, fixed-temperature boundary conditions, heat loads, heat fluxes, and orbital heating are candidate boundary conditions that the analyst considers.

Reliable operation of the optical system necessitates that thermal requirements are met throughout the mission; therefore a thermal-control scheme is devised. Passive and active thermal-control hardware ensures that the proper amount of heat transfer occurs. Examples of thermal-control methods include MLI, surface finishes, heaters, and radiators. MLI is an illustration of a passive method used to minimize heat absorption or rejection in certain areas. Heaters provide active thermal control to compensate for wide ranges of internal and external heat inputs. Because these components are typically not modeled by the structural designer, the thermal analyst may add FEM meshes or thermal couplings for such items.

Modeling the space environment to which the optical system is exposed is accomplished by specifying an orbit definition. Based on the altitude and orientation of the spacecraft, I-DEAS/TMG calculates the environmental thermal load generated by solar heating, Earth albedo, and Earth-emitted infrared (IR). Depending on whether results of steady-state or transient behavior are desired, solver parameters are set and temperatures are calculated using I-DEAS/TMG's finite-volume formulation.

For the representative space optical system, the thermal analyst begins by defining the environment to which such a system is exposed. For this system, the mirrors view deep space and the surrounding payload structure, which is covered with MLI. A radiation parameter is specified in I-DEAS/TMG to simulate the radiative heat transfer from the optical system to cold space. A temperature boundary condition and emissivity properties are established to represent the MLI on the

payload structure. The Zerodur mirrors must maintain room temperature to take advantage of the near-zero CTE. To achieve this condition, radiant heaters are placed behind the mirrors and a heat-load boundary condition is created, identifying the power required. The mirror sides and rear are then covered with MLI to reduce heat loss. A steady-state analysis is performed accounting for conductive and radiative heat transfer. Figure 17.9 shows the temperature distribution of the system. (Because the purpose of this section is to discuss methodology rather than specific results, no temperature values are shown.)

Structural Analysis

Using the thermal-analysis temperatures as boundary conditions, the analyst performs a thermal deformation on the system. As noted in the meshing section, a utility within I-DEAS/TMG is available to map temperatures from one mesh to another in cases where unique meshes are created by thermal and structural analysts. Care must be given to the global coordinate system of the two meshes—the target model must be oriented identically to the thermal model. Also, I-DEAS must be set to the same global measurement units in which the thermal model was solved.

Once the temperatures are associated with the structural mesh, additional mounting constraints are created using I-DEAS's Boundary Condition module. In high-precision optical systems, kinematic mounts are utilized to prevent additional distortion of the optical elements, which may occur because of changes in the mounting force resulting from thermal deformations. The advantages of kinematic mounts are increased stability, distortion-free optical mounting, simplicity, and low cost.^{17.3,17.4} To model kinematic mounts, all six degrees of freedom (three translations and three rotations) of the optic are constrained in a manner that allows the optical element to freely deform without experiencing any external force (i.e., stress).

Given the temperature boundary conditions and the mounting restraints, the thermal-deformation model is solved using the I-DEAS Model Solution module.

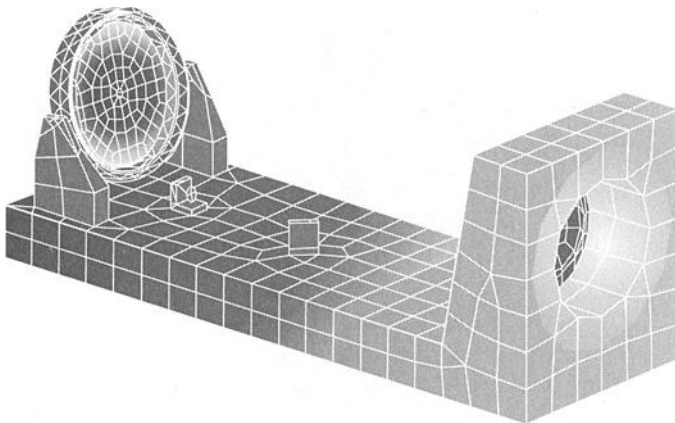


Fig. 17.9. Temperature distribution of a space optical system.

The surface nodes for each optical surface are then grouped, and their initial locations and displacements are exported to an I-DEAS Universal file format. This format is often used for transferring data between users of I-DEAS or other software programs such as OPTIMA.

To streamline demonstration of the methodology, the thermal-analysis FEM mesh is used for the deformation analysis. Using the computed temperatures and assuming a kinematic mount, Fig. 17.10 shows the resultant thermal deformation of the siderostat mirror. (Note: The deformation of the mirror is exaggerated to show detail; however, no actual results are displayed, because the focus is limited to the modeling process.) The surface nodes of the mirror with their original coordinates and displacements are then exported to an I-DEAS Universal file for transfer to the optical analyst.

Optical Analysis

Once the displacements are known, they are transferred to the optical designer, via Universal file, to characterize their impact on the image quality. No translation of coordinates is necessary, because the optical designer established the coordinate system in the first phase of the process. Utilizing OPTIMA, the optical analyst creates Zernike polynomials to represent the distorted surface and evaluates the optical performance. On the basis of the results from this process, the optical designer may propose design changes. If necessary, the process is repeated until a satisfactory design is established.

Several benefits are thus realized, including increased precision and prevention of duplication. These benefits are gained by taking advantage of a single material database for all analysis routines and sharing a common software environment for much of the analysis and design. Additionally, the methodology enables individuals

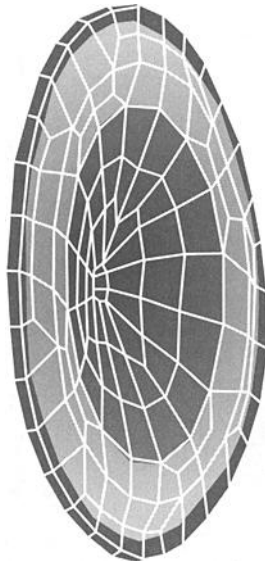


Fig. 17.10. Thermal deformation of siderostat mirror.

from various disciplines to work together, rather than in isolation, much earlier in the product-development process, reducing time to market.^{17.5}

Test Verification

A thermal-vacuum test was conducted on a simulated SIM primary mirror to verify the ability to perform milliKelvin-resolution temperature measurements and to assess the measurement-system uncertainties. The thermal-modeling tools and approach were also validated by correlating the temperature-difference measurements in the mirror to predictions over a range of conditions, including small perturbations consistent with those allowable during flight science-observation periods.

The test was conducted on a 33.5-cm-diameter plano mirror under conditions of small thermal perturbations that induced steady-state temperature gradients of 10 to 100 mK. Tests were performed with small heat inputs to the back of the mirror, which was suspended in a thermally uniform shroud. Correlation of thermal models for both conductively and radiatively heated test configurations were performed, and results indicated very good agreement between the thermal-model predictions and the temperature measurements. After adjusting the model to match the known initial temperature indicated by the test data, the analytical uncertainty in predicting subsequent temperature changes from the initial condition was found to be on the order of ± 3 mK.

Test Configuration

The test configuration used is shown in Fig. 17.11. A cylindrical copper shroud (91 cm long by 3.2 mm thick, with a 74-cm diam) sat on four fiberglass supports inside the vacuum chamber. The shroud was covered with a 20-layer blanket to radiatively isolate it from chamber-wall temperature fluctuations. It was painted black (Chemglaze polyurethane) on all interior surfaces to provide a high, uniform emittance and a uniform temperature. The test article was suspended in the copper shroud via 2.5-mm-diam Kevlar twine with end loops. Threaded eyes were used to

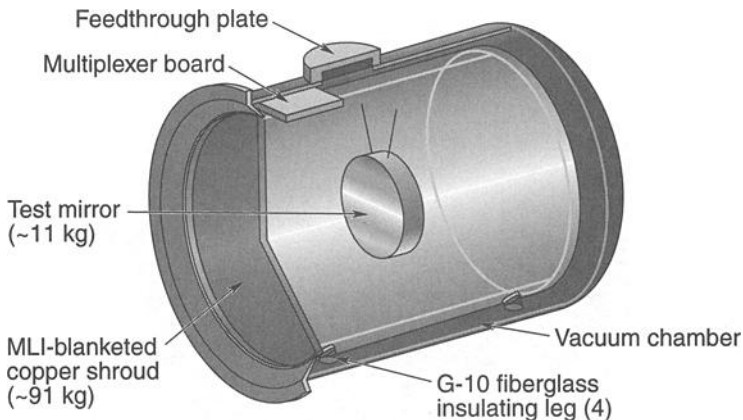


Fig. 17.11. Overall test configuration.

attach the lines to the shroud and the test article. The test article was heated to induce small temperature gradients that were measured using a high-accuracy sensor system.

The test article was a 33.5-cm-diam, 5-cm-thick Pyrex plano mirror, polished and coated with protected silver (Denton) on the front surface. The mirror had 22 small (1.1-mm diam, 8 mm deep) holes drilled into it for sensor installation, and two larger holes (9.5-mm diam, 31.8 mm deep) for installation of mounting hardware. The sensor hole locations are illustrated in Fig. 17.12. Note that the edge sensor holes are in a spiral pattern to allow axial and circumferential resolution. Small threaded invar plugs were epoxy-bonded into the mounting holes. The Kevlar support lines were attached to screws threaded into these plugs.

Two methods of heating the test article were used, conductive and radiative. Both used a 1-mm-thick, 33-cm-diam, 500- Ω nominal resistance, adhesive/foil-backed Kapton heater with embedded nichrome wire elements (7.2-mm spacing).

Calibrated miniature platinum resistance thermometers (PRTs) were installed at the 18 embedded locations on the mirror shown in Fig. 17.12. The locations were designed to show axial and radial temperature distributions in the mirror, while minimizing the impact of the sensor holes on the mirror temperature distribution. To obtain temperature measurements of sufficient accuracy for this project, a special measurement system was utilized to obtain measurements from the PRTs. The readout system consisted of a Linear Research KR-700 AC Resistance Bridge, a custom in-situ multiplexer to allow serial measurements, and a PC-based National Instruments data-acquisition system. The PRTs were specifically calibrated using this system in 5°C increments over the 15–40°C temperature range. The system attains relative accuracy (defined as the difference between different sensors when they are at the same true temperature) of ± 1 mK, when sensors are undisturbed following calibration.^{17.6}

Following instrumentation and heater attachment, the back and sides of the mirror were covered with MLI as shown in Fig. 17.12.

Test Results

Following establishment of a quasi-steady-state condition, the power input to the heater plate was incremented in steps of 10 or 20 mW. This case was intended to

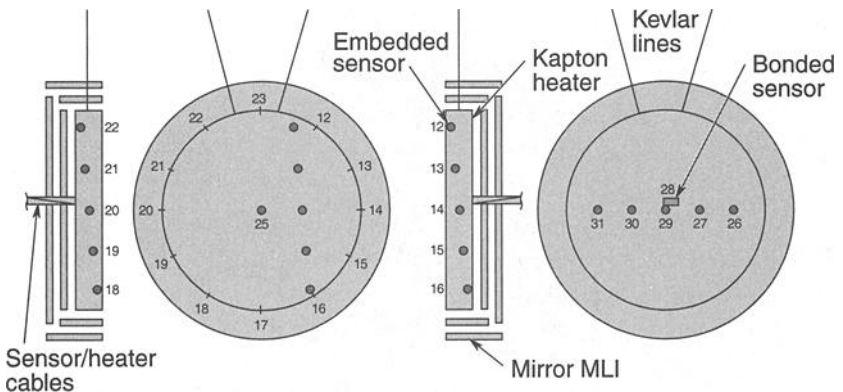


Fig. 17.12. Test mirror layout.

simulate the small thermal-environment perturbations predicted for the flight conditions. The changes in the centerline and edge gradients for the 20 mW transient step power change are shown in Figs. 17.13 and 17.14.

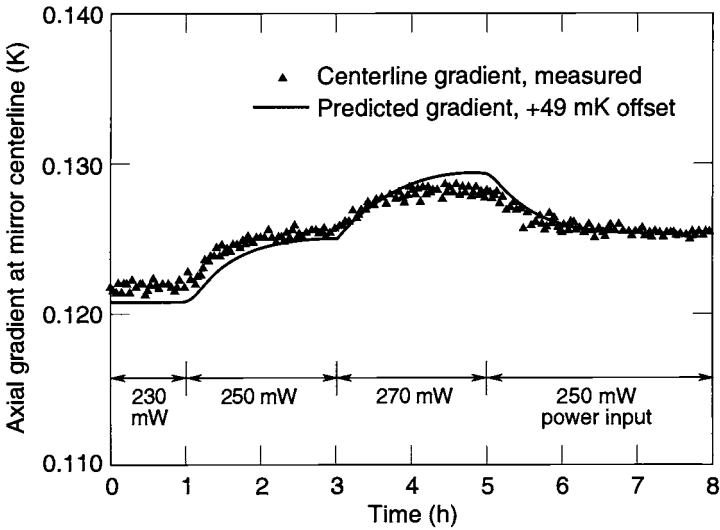


Fig. 17.13. Centerline gradient for 20 mW transient step power change.

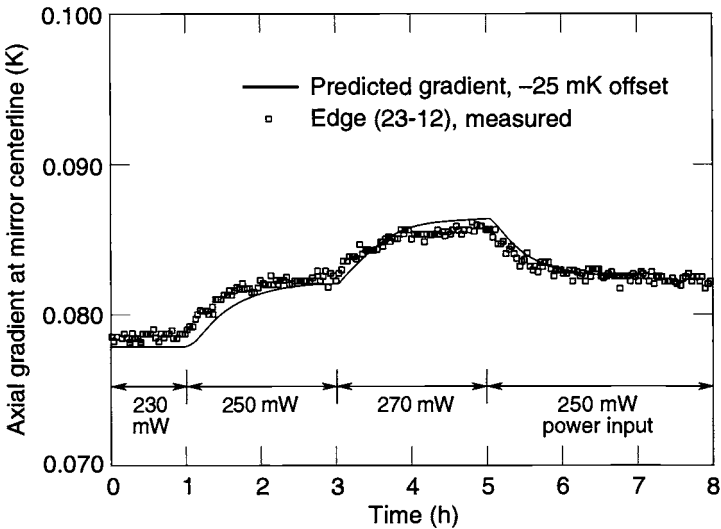


Fig. 17.14. Edge gradient for 20 mW transient step power change.

Thermal Model Description

The thermal model for test correlation was generated in I-DEAS/TMG.^{17.7} The basic configuration is shown in Fig. 17.15; it consists of the mirror, heater or heater plate, mirror MLI, shroud, Kevlar lines, and cable bundle. The boundary conditions are:

- fixed, constant shroud temperature
- fixed temperature at Kevlar line ends (same as shroud)
- fixed temperature at cable bundle end (same as shroud)
- fixed heat load on heater or heater plate

The mirror submodel, shown in Fig. 17.16, consists of 3096 solid elements with 258 shell elements on the front and back faces and 624 shell elements on the cylindrical side surface. The mesh size was selected to provide a resolution consistent with the sensor spacing along the edges in the mirror axial direction (12 layers through-thickness). The size of the elements (average face-shell element of 342 mm²) is substantially larger than that of the sensors (~2.5 mm² normal to the face). This contributes an uncertainty to the comparisons between specific element temperatures and sensor measurements.

The mirror MLI was modeled using zero-thickness elements with a much coarser mesh. There are 44 shell elements representing the MLI back surface and 40 shell elements for the edges and front-edge section. The cable bundle (2 elements) and Kevlar lines (4 elements each) were represented using beam elements.

Radiative view factors were calculated in I-DEAS/TMG for an enclosure consisting of the MLI external surfaces, the mirror front face, the shroud internal surface, and the cable bundle and Kevlar line beam elements. All surfaces were assumed diffuse for radiation calculations. The mirror shell elements beneath the MLI were thermally coupled to the MLI with radiation conductors. These are based on the primary element (mirror) area and a multiplying factor used to represent the MLI effective emittance.

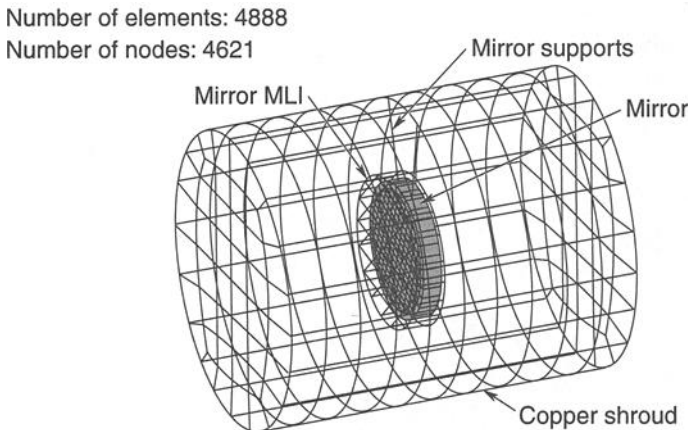


Fig. 17.15. Thermal model for test correlation.

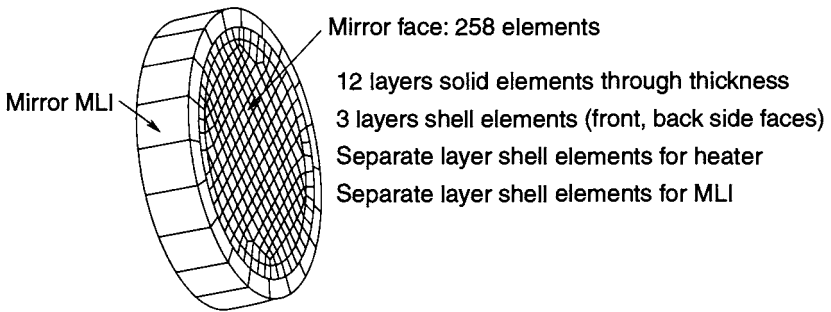


Fig. 17.16. Mirror submodel.

Results Comparison

Model correlation consisted of varying the thermal parameters to obtain the best match to the quasi-steady-state data. The model was then used to predict transient through-thickness gradient response. This value is considered to be of primary importance to meeting the SIM instrument-performance requirements. The MLI effective emittance is subject to much greater uncertainty than all other parameters. This is a result of both the large degree of uncertainty in the fabrication process and the empirical nature of the effective-emittance model used to predict performance. Uncertainties in MLI performance prediction of 50–100% are typical. Emittance of the mirror front surface is second in order of uncertainty, as shown by the measurements performed on the coating witness samples. Emittance of the MLI external surface is probably of an order similar to that of the mirror coating, but the results are less sensitive to this parameter. Other parameters considered to be less uncertain are the shroud internal coating emittance, mirror thermal conductivity, and mirror specific heat; the mirror temperature distributions are relatively insensitive to the range of values assumed.

The predictions for axial mirror temperature gradient were compared. The measured and predicted centerline axial temperature gradients for the 20-mW step power change are shown in Fig. 17.13. The measured and predicted edge axial temperature gradients for this same case are shown in Fig. 17.14. For convenience, these predictions assumed a constant shroud temperature. The measurements show that the shroud temperature varied by approximately ± 150 mK during the period of interest. The transient behavior of the predicted gradients was found to match the measured values very well, with an agreement of approximately ± 1 mK. The absolute gradient values differed by 25–50 mK. The predicted gradient values have been offset by the amounts shown to match the starting value of the gradient.

The Hydrogen Maser Clock

Frequency references—high-stability clocks—increasingly find applications in space missions. Atomic clocks of ever-increasing stability have present and potential uses as frequency references for Global Positioning System navigation satellites and for detection of gravitational radiation, local oscillators for space-based

Very Long Baseline Interferometry, “proper” clocks for tests of general relativity, and “traveling clocks” for worldwide time transfer.

An active atomic hydrogen maser for long-term use in space has been designed and built as part of the Smithsonian Astrophysical Observatory’s HMC project. HMC is a NASA-sponsored program whose goal is to produce and demonstrate a space-qualified hydrogen maser with drift-removed fractional frequency stability of 10^{-15} or better in one day. Achieving such stability requires very precise temperature control. The HMC maser and its control electronics have been designed as an integrated system for use on a variety of spacecraft, requiring only an appropriate mechanical connection and electrical interface. It is an evolutionary outgrowth of a two-decade program of research and development of hydrogen masers for Earth and space use.

Mechanical and Structural Characteristics

The HMC maser’s physics unit, shown in cross section in Figs. 17.17 and 17.18, takes the general form of a cylinder 84 cm long and 43 cm in diameter. The maser’s main components are: a quartz storage bulb and low-expansion resonant cavity; the titanium vacuum tank that contains the cavity; vacuum manifold and source for producing a beam of hydrogen atoms; electrical heaters and thermistors for thermal control; and components for magnetic-field control. Separate electronics units contain analog and digital control and monitoring circuits and a microprocessor that controls the maser’s electronics and acts as an interface with the spacecraft’s data and command system.

The maser is supported structurally from a circular aluminum midplane plate, with its resonant cavity and vacuum tank on one side and its vacuum manifold and hydrogen source on the other. The midplane plate is the main structure for mounting the maser to the spacecraft. Two titanium tubes connect the vacuum tank to the midplane plate at the bottom end and to the maser’s cylindrical outer aluminum housing at the top. The housing, in turn, transfers the upper tube’s load to the midplane plate.

Thermal-Control System Design Features

Temperature changes of the maser’s resonant cavity and storage bulb affect the maser’s output frequency. To stabilize frequency the cavity temperature must be maintained constant to approximately 0.1 mK for more than a day. The HMC maser employs several strategies to achieve this level of temperature control. The integrated system is of particular interest because it embodies a large number of elements common to precision active thermal control for the space environment.

To control heat flow from the vacuum tank, the maser’s structure is divided into three concentric isothermal control regions, or zones. Each region establishes the external environment of the next-inner region. If we assume the external environment varies roughly $\pm 10^\circ\text{C}$, then each control zone must attenuate this variation by a factor of 50 to achieve the desired accuracy of maser thermal control. Thermal gradients are controlled by subdividing each isothermal region into multiple independently controlled zones, by mounting controlled guard heaters on heat-leakage paths, by separating heaters from the primary controlled structure (the vacuum tank), and by carefully calibrating and matching thermistors and set-point

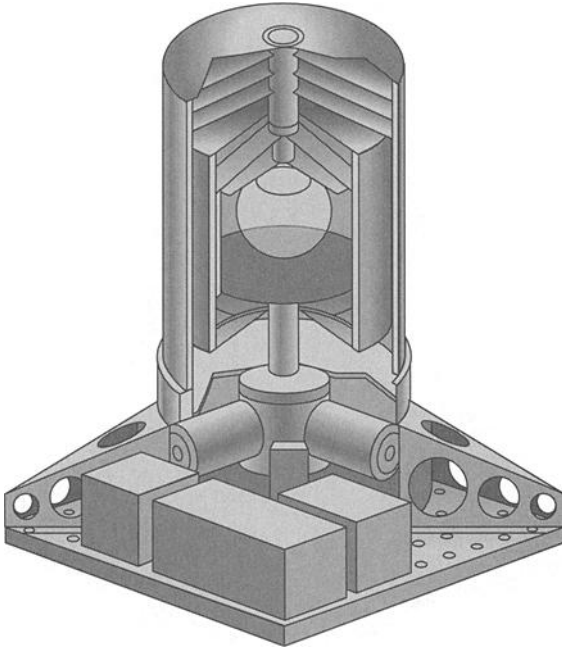


Fig. 17.17. The HMC.

resistors to ensure that all zones of an isothermal control region are at the same temperature. Radiative heat flow is controlled by surface emittances and selective use of MLI in the evacuated annular spaces between the regions, while conductive heat flow is controlled by design of the segmented nylon magnetic-shield support rings and interface materials and bolting pressures. The control-system configuration is entirely axial and radial; no side-to-side or circumferential control is used. External MLI was found to be adequate to isolate the package from typical satellite internal thermal environments.

As shown in Fig. 17.18, the innermost isothermal region, the titanium vacuum tank that surrounds the resonant cavity, is maintained at 50°C . The resolution of the tank control system is 0.1 mK . To reduce thermal gradients in the tank, the three tank heaters are separate from the tank itself, one located on the outside surface of the inner magnetic shield that is directly outside the tank and the others on the titanium tubes where they support either end of the tank.

The tank, in turn, is surrounded by a 40°C aluminum shell located directly over the third magnetic shield. This oven region acts as a guard to control heat that flows from the tank region both radiatively from the tank surface and conductively along the magnetic-shield supports and the titanium support necks. The oven region consists of three control zones located on the cylinder and two end surfaces of the oven, and two zones mounted on the outer ends of the support necks.

The third isothermal region consists of the midplane plate and an outer aluminum support shell that directly surrounds the fourth magnetic shield. This zone is

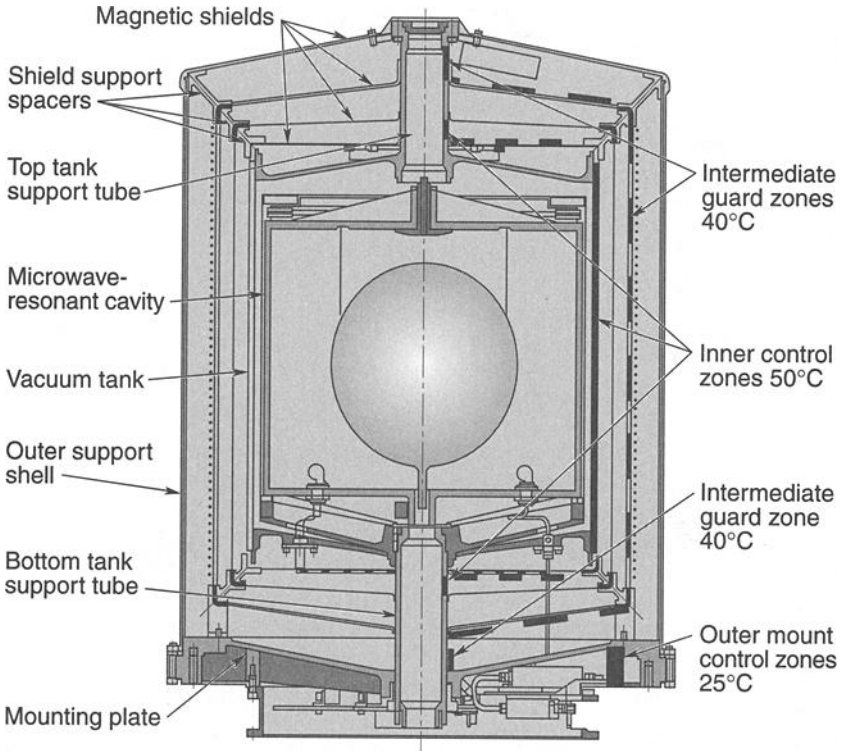


Fig. 17.18. Design elements and thermal zones of the HMC.

maintained at approximately 25°C by a control thermistor and heaters mounted on the midplane plate.

In addition to the thermal-control zones that are integral to the maser, the system includes a controlled-temperature guard station on the structure that mounts the maser to the spacecraft, to act as a first stage of isolation from the conductive environment. The entire instrument is surrounded with MLI to isolate it from the radiative environment.

Early trade-off studies established the major design choices in the thermal-control system. Highly stable thermistors were chosen over wire-wound thermal sensors to minimize effects of lead-wire resistance. Each zone has two identical thermistors, one for control and one for monitoring (which can replace the control unit if necessary). Proportional/integral control was selected to eliminate proportional-offset control error, and digital control was picked over the more conventional analog to decrease thermal effects on controller circuits and for ease in modifying loop gains and time constants. Kapton-insulated etched-foil heaters were chosen to reduce magnetic effects; in critical regions a specially designed “sandwich” of two identical elements with opposing currents was needed to ensure the lowest possible magnetic-field generation.

The thermal-control system incorporates several electronic and hardware features to achieve the required high degree of thermal stability. The digital electronic control system is based upon 68HC11 microcontrollers, each of which can control up to five thermal zones. Each 68HC11 includes a microprocessor, an 8-bit analog-to-digital converter (A-to-D) with eight-channel multiplexer, and timer registers that are used as pulse-width modulators driving a power stage for high-efficiency switched heater power control. The vacuum-tank heaters closest to the maser's resonant cavity are driven at high frequency (4 kHz) to avoid perturbation of the maser oscillation; the other heaters are switched at a 30-Hz rate. The thermal-control program provides for differential control as well, but this additional algorithm term is primarily useful in startup dynamics and has been found unnecessary. Temperature set-point resistors have low temperature coefficients, and are physically mounted on a temperature-controlled zone within the maser for minimum temperature perturbation.

High-Precision Control Considerations

Thermal control at milliKelvin stability levels requires integrated design of thermal, mechanical, and electronic hardware. Effects that are negligible in conventional thermal control must be addressed systematically and their impacts allocated and traded for performance. Figure 17.19 shows a schematic of the control system with the most important elements labeled. A discussion of some of the important system issues is useful, because they apply to a wider class of high-precision control systems, especially those under digital control.

Control Loop

The offset error can usually be controlled by integral compensation, except during transients. It is important to use an algorithm that does not increment the integral

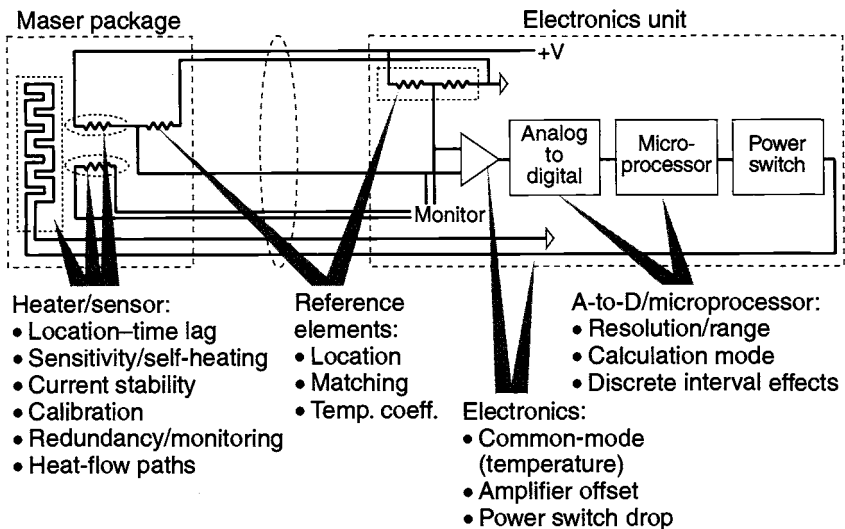


Fig. 17.19. HMC heater-control system.

when the temperature error is large, certainly not beyond the proportional band. The cycling period and heater/sensor time lag are closely related; the control sensor should be located as near the heater as possible, especially on poorly conducting substrates. Separating the natural cycling frequencies of adjacent zones is preferable, to prevent interaction.

Heater Power and Location

Good practice dictates that the heater should be well matched to the power requirement, and this is particularly true when the driving voltage is pulse-width modulated digitally. If, for example, the pulse width has 256 possible values, a heater operating at 50% duty cycle has a minimum power change of just under 1%. If the heater is oversized so that it operates at 8% duty cycle, the minimum power resolution is about 5%. This raises the effective system gain and can cause hunting or cycling. Heaters should be located so that power changes in response to the control loop do not induce thermal gradients in the most critical control zones; heat should flow primarily outward from each heater.

Sensors

Sensors were individually calibrated in an oven at the control temperature so that the set points could be corrected to minimize gradients in the vacuum-tank zones. If sensors are well matched, averaging more than one may be effective. On HMC two identical sensors were installed side-by-side for redundancy; one was used for independent monitoring of zone temperature, but it could be used for control in case of failure. Self-heating is significant—the self-heating constant of sensors cemented to the controlled surface was measured at about 150 mK/mW, and they are operated at about 0.3 mW. This yields a self-heating temperature rise of nearly 50 mK, which means that the current stability in the sensor must be good enough for the self-heating changes to be much smaller than the control resolution. In the future, consideration should be given to using narrow current pulses for sensors to reduce self-heating. Also, the sensor time constant was a significant contributor to the natural frequency in the HMC control loops.

Reference Elements

At the milliKelvin level, temperature effects on the fixed resistors in the control bridge can be significant. HMC located the set-point resistors in one of the controlled zones, and used a single-substrate matched resistor pair in the electronics unit for the other side of the bridge.

Cables can produce significant noise with microvolt-level signals. Noise is evident on the low-level error data and makes monitoring difficult. Shielding can be effective, but wiring in inner parts of the HMC left no space for it. Noise is not necessarily bad in the control loop as long as it averages to zero—but assurance of this is seldom available.

The instrumentation amplifier can have an input voltage/current offset that is temperature dependent, and that impresses electronics-unit temperature changes on the control circuit. Careful design is needed; using a pulse train on the temperature-sensing bridge may also eliminate the problem.

The A-to-D creates a basic trade-off in design: resolution versus range. HMC used an 8-bit A-to-D (256 values) in the control loop; for a minimum resolution of

0.1 mK, the total range was only 25 mK. This implies a very high gain; dynamic control is a potential problem, and control points must be set very carefully. A variable gain may be incorporated in future units: high near the set point for good resolution and lower elsewhere for increased range. The digital processor has a choice of integer vs. floating-point arithmetic. Integer arithmetic is faster and uses less memory, but control algorithms must be developed carefully to ensure that critical information is not lost in truncation.

The transistor power switch has a voltage drop that is temperature-sensitive. An increase in switch temperature decreases voltage to the zone heater and requires the control system to compensate. The same effect would occur with a variable bus voltage. Removing as many disturbances as possible is usually best, especially for high-gain loops. A secondary loop was considered (but not implemented) to compensate for heater voltage; this could be important for a system with wider voltage changes.

Thermal Analysis

A thermal mathematical model of about 100 nodes supported design and test of the HMC. This model's purpose was twofold: prediction of heater power requirements (rather than temperatures, which were controlled) for each of the zones, so that adequate control margins could be established, and study of some changes in design parameters (heater location, for example) to minimize critical gradients. The model, with the control-zone configuration, had only axial and radial detail. Each concentric shell—vacuum tank, magnetic shields, oven, and outer shell—was divided into six zones axially and three radially (each end). Individual surface emittances were maintained as independent parameters so that they could be used to “tune” the heat-flow paths.

Modeling the conductive paths was particularly difficult because of the large number of contact resistances with low interface pressures. The magnetic shields, for example, have end caps that are a slip-fit over the cylinders, and the surfaces have low measured emittance. These shields are held in place with padded nylon spacers because the strains induced by conventional fasteners would affect shielding properties. Interfaces between the titanium support tubes and the top and bottom structural supports, two primary heat-flow paths, have very small areas and insulating spacers. The top support-tube interface was in fact the primary area of “disagreement” between model and hardware. Thermal isolation in this path was considerably greater than expected, effectiveness of that guard heater was less than desirable, and the top oven-guard power was higher than expected.

Table 17.1 shows predicted and actual heater power and installed capacity for each zone. Control power predictions are acceptably close to measured values, indicating that use of the model to minimize heat flow and gradients in each zone was probably successful. Operating a control zone in the steady-state condition at about one-third to one-half its maximum range is desirable to allow upside and downside control margins and warm-up capability, and we achieved this goal for most control zones. The design provided for a choice of two voltage levels to drive the most critical zones in case predictions were greatly in error. Two zone-heater voltages were changed after initial test: the upper guard tube voltage was decreased

Table 17.1. Predicted, Actual, and Maximum Heater Power

Control Zone	Heater Power (W)		
	Predicted	Actual	Maximum
Support guard top	2.1	0.8	1.7 (was 6.6) ^a
Vacuum tank top	0.5	0.4	1.5
Vacuum tank radial	0.8	1.1	5.8 (was 1.3) ^a
Vacuum tank bottom	0.9	0.8	1.5
Oven guard top	0.2	0.6	2.5
Oven guard radial	1.4	2.9	4.2
Oven guard bottom	2.0	1.9	2.5
Support guard bottom	4.0	2.6	6.6

^aValue was changed after testing, see text for explanation

because of the high thermal resistance path discussed above, and that of the tank radial zone was increased because measured power had little margin.

Tuning and Experimental Verification of the Thermal Design

The experimental portion of the HMC program had the dual goals of tuning the individual zones for best control performance and then evaluating both thermal performance and frequency of the clock under reasonable changes in external environments. Both tests were conducted in a vacuum tank, because gas-conduction effects would produce very different control results under ambient conditions. Changes in both the radiative environment on the outer-shell MLI and the conductive sink temperature were expected in the mission environment, so two fluid loops were incorporated in the test fixture, one surrounding the shell and the second at the mounting interface. In a near-Earth mission environment these environment changes would have a primary period of about 1.5 hours, which was difficult to simulate in the laboratory, so the primary focus was on the more severe case of measuring step response and inferring control performance from those measurements. This test was regarded as a reasonable simulation of a carrier vehicle maneuver that could significantly change solar exposure, for example.

The control loops were tuned using a classical method^{17.8} that requires removing all integral/differential compensation and increasing linear loop gain until the temperature oscillates at a constant amplitude. Gain is then reduced and integral compensation added in a related amount to produce a slightly underdamped response to a step change. Control response was observed according to a classical rule of thumb that states that the primary oscillation is usually determined by the shortest lag or time constant in the system. Most of the high-gain loops oscillated with a 5–10-second period, which is likely related to the thermal lag between the heater mats and the adjacent control thermistors (measured at 1–3 seconds), and probably dominated by the 2-second thermistor time constant. In addition, the zones at either end of the vacuum tank, though locally identical mechanically and

in fabrication, were observed to have quite different control parameters when tuned properly. This emphasizes the need to retain flexibility in thermal-control system design to accommodate the effects of small but important variables in the as-built (versus design) configuration.

The similarity in natural frequency of adjacent control zones gave rise to concern about possible dynamic interaction between zones—the oscillatory response of a guard zone could induce a similar oscillation in an inner zone. This was tested by manually varying the set point of a guard zone at the observed frequency of the adjacent vacuum-tank zone, and no effect was observed. Evidently the combination of conductive damping and integral compensation is adequate to isolate the inner zone. Control system performance was tested by observing the amplified control-bridge null signal, the monitor thermistor resistance, and the heater output of critical control zones in response to environmental changes. Corresponding changes in maser frequency stability were also sought, although this was more difficult because of the known time lag and the presence of small perturbations in frequency from other sources. The approach to frequency-stability measurement was to make an environmental step change on one day and an offsetting change on the succeeding day, and look for a one-day offset response.

Sample Performance Results

Figure 17.20 illustrates an example of performance data recorded during a 2-1/2-day period of laboratory environment changes. The temperature of the surrounding environment was intentionally allowed to vary about 10°C. Temperature of the

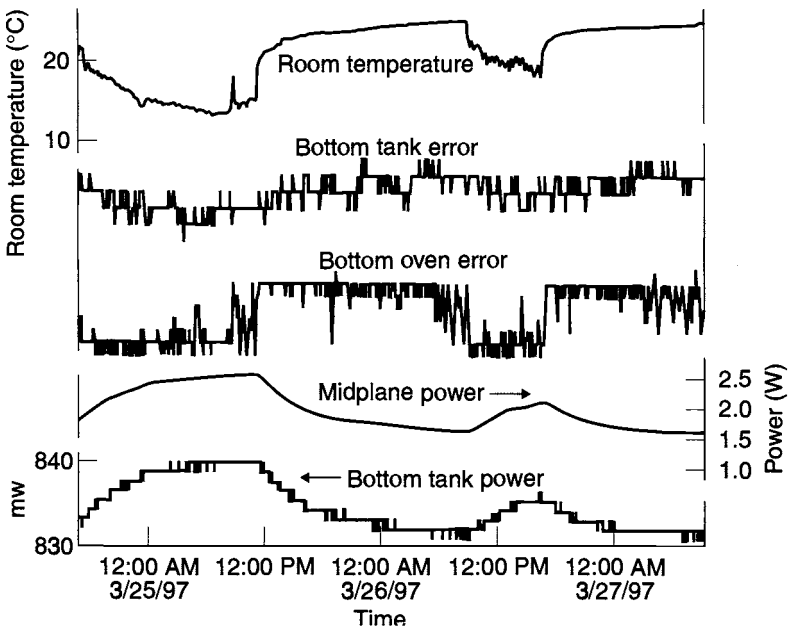


Fig. 17.20. Effect of external environment on control stability.

controlled zones is represented by the error signal from each sensor bridge. The midplane isolation zone sensor was held to less than a 10-mK variation with a power change of 60%. (With such a large power change, we certainly expected substantial gradients in the mounting plate, but we had no sensors with which to verify this expectation.) The bottom oven and neck guard zones, which control both conductive and radiative losses to the midplane zone, were stable to a fraction of a control resolution element (about 5 mK for the oven, below the threshold of measurement for the neck) with 7–9% power change. The adjacent inner tank zone was stable to a few parts in 0.01 mK with power variation a little more than 1% peak-to-peak. Relative power variations are an indirect measure of the degree to which the critical zones are isolated from the outside environment.

Figure 17.21 shows performance of an innermost zone when the adjacent guard zone is changed by a large amount. For this test the guard-zone control set point

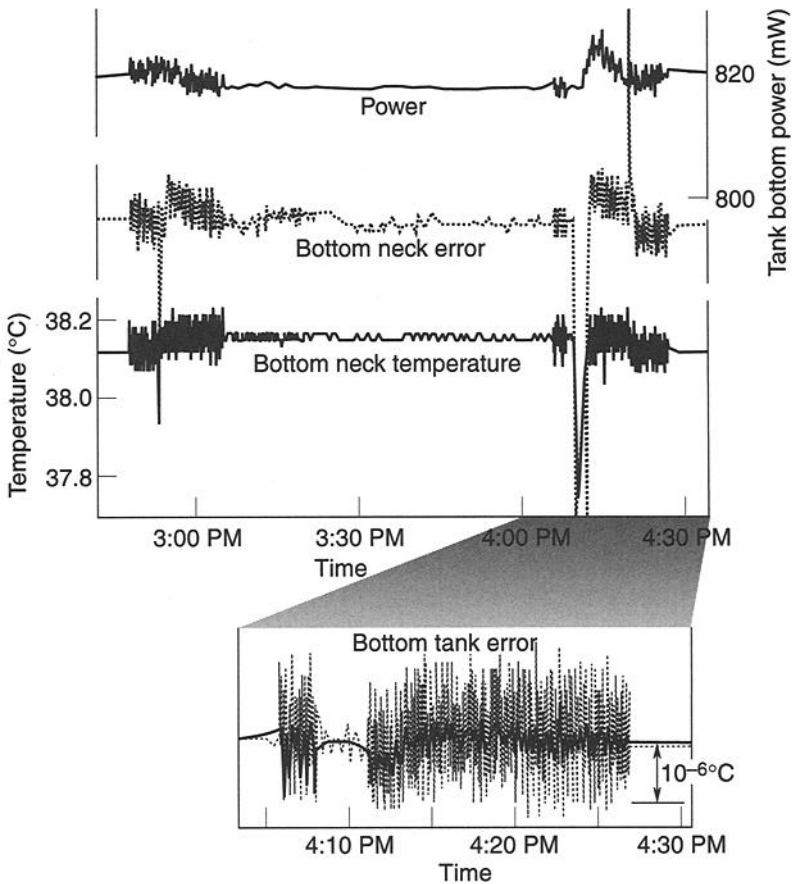


Fig. 17.21. Effect of guard zone on adjacent control-zone response.

on the bottom neck was increased by 30 mK (30 times its control band) for about an hour, then returned to its original setting (top trace; discontinuous data shows the digital measurement resolution, and the trace envelope indicates data noise that changes with sampling period). The bridge error of the guard zone (second trace) shows clearly the settling transients after each adjustment, with a peak-peak amplitude less than 10 mK. The critical zone is the vacuum-tank bottom; its power (third trace) decreases by about 0.3%, roughly the same as the temperature difference between its set point and that of the adjacent guard zone, and shows a 1% spike on resetting. The last trace expands the time scale of the control-zone error for the second (resetting) transient, and shows zero offset at 0.01-mK resolution across the transient. The peak-peak temperature error, noise included, lies within 0.3 mK even while the integral compensation drives the power transient, with a noise-corrected span (dark trace) within a 0.1-mK band.

Common-mode effects of electronics-unit temperature change are illustrated in Fig. 17.22. Electronics temperature was abruptly raised by about 10°C and decreased by 15°C two days later. The error signal from an internal tank zone barely shows change at the 0.01-mK level, but the indicated temperature measurement from an adjacent sensor appears to change by about 50 mK, well correlated in time with the electronics-unit changes. The monitor circuit is not designed for high-precision measurement but for telemetry over a wide range, and the relative response of the two measurements indicates the degree to which the control system is successfully isolated from common-mode effects.

HMC Test Program Conclusions

The laboratory test program of the HMC has confirmed the ability of the thermal-control system in the presence of varying environmental conditions both to maintain

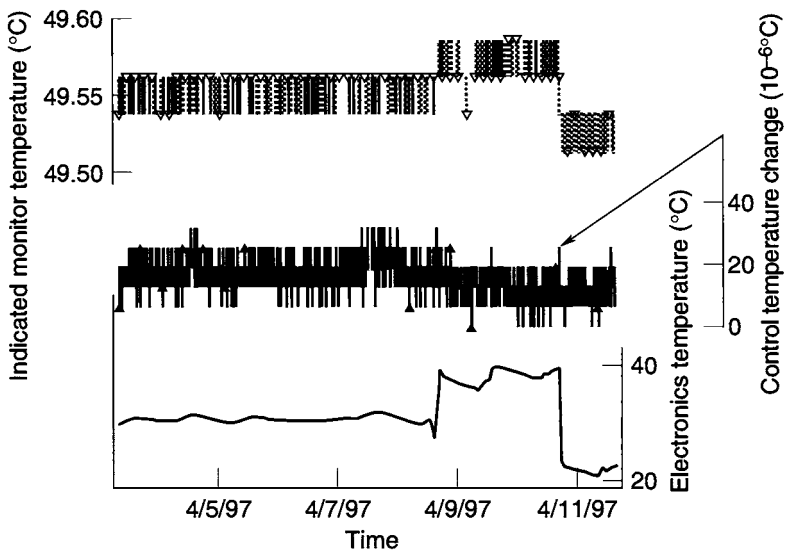


Fig. 17.22. Effect of electronics temperature on monitor and control.

internal-zone temperature stability to considerably better than 0.1 mK at the control sensors, and to attenuate control power changes. Of course, stability of control sensors must be distinguished from overall zone stability. A guard-zone power change of 7–9% surely induces some gradients, and a 1% inner-zone power change is a response to this guard-zone nonuniformity. Successful separation of dynamic response of zones was demonstrated.

The discrete nature of microprocessor-based control was not seen to degrade high-stability control performance, and its advantages in ease of optimizing system performance make it highly recommended for applications such as HMC.

While long-term stability at the submilliKelvin level was not a design issue for HMC, changes that would enhance long-term stability have been indicated. Other aging effects would need to receive the same design attention that has been illustrated here.

Summary

Despite the seemingly enormous challenges involved, maintaining temperature stability on the order of milliKelvins or better appears possible with the same basic techniques of heaters, MLI, low-emittance surfaces, and low-conductance mountings that are used in most other thermal designs. However, as the HMC experience illustrates, implementation of heaters for active control of temperature to the milliKelvin level is much more complex than for heaters in more conventional spacecraft applications. For instruments that must be exposed to the surrounding environment, such as the SIM payload, special orbits may also be required to eliminate variations in heat loads resulting from eclipses or changes in Earth-emitted IR or albedo.

References

- 17.1. K. Aaron, D. Stubbs, and K. Kroening, "Space Interferometry Mission Instrument Mechanical Layout," paper no. 319, IEEE Aerospace Conference, Big Sky, 2000.
- 17.2. K. Aaron, D. Stubbs, L. Ames, and T. Kvamme, "Space Interferometry Mission: Recent Instrument Configuration Developments," paper no. 020, IEEE Aerospace Conference, 2002.
- 17.3. D. Vukobratovich, "Introduction to Optomechanical Design," SPIE In-Company Customized Course in Optics and Potonics, Course Notes, May 1997.
- 17.4. D. Vukobratovich, D., "Advanced Topics in Opto-Mechanics," SPIE In-Company Customized Course in Optics and Potonics, Course Notes, October 1997.
- 17.5. J. Pecson and A. Hashemi, "Multidiscipline Analysis for Space Optical Systems," AIAA 2002-0358, 40th AIAA Aerospace Sciences Meeting & Exhibit, Reno, NV, January 2002.
- 17.6. J. Ambrose, A. Hashemi, J. Schneider, D. Stubbs, K. Aaron, M. Shao, and T. VanZandt, "Measurement and Prediction of Temperature Distributions in Optical Elements in the MK Regime," HTD-Vol.366-5, pp. 135–145, IMECE 2000, Orlando, FL, November 2000.
- 17.7. MAYA Heat Transfer Technologies, Ltd., I-DEAS Master Series 7 Course Guide, The Advanced TMG Course Manual, August 2000.
- 17.8. J. G. Ziegler and N. B. Nichols, "Optimum Settings for Automatic Controllers," *Trans. ASME* **64** (8), 1942.